DISCLAIMER

This report was prepared as an account of work sponsored by an agency of the United States Government. Neither the United States Government nor any agency thereof, nor any of their employees, makes any warranty, express or implied, or assumes any legal liability or responsibility for the accuracy, completeness, or usefulness of any information, apparatus, product, or process disclosed, or represents that its use would not infringe privately owned rights. Reference herein to any specific commercial product, process, or service by trade name, trademark, manufacturer, or otherwise does not necessarily constitute or imply its endorsement, recommendation, or favoring by the United States Government or any agency thereof. The views and opinions of authors expressed herein do not necessarily state or reflect those of the United States Government or any agency thereof. Reference herein to any social initiative (including but not limited to Diversity, Equity, and Inclusion (DEI); Community Benefits Plans (CBP); Justice 40; etc.) is made by the Author independent of any current requirement by the United States Government and does not constitute or imply endorsement, recommendation, or support by the United States Government or any agency thereof.

INL/RPT-25-82868

Nuclear Energy Advanced Modeling and Simulation Program

Leveraging MARVEL And SPHERE To Demonstrate NEAMS Thermal Hydraulics Codes

DECEMBER 2024

Joshua E. Hansel,
Vasileios Kyriakopoulos, and
Lise Charlot

Idaho National Laboratory

Idaho National Laboratory

Battelle Energy Alliance manages INL for the U.S. Department of Energy's Office of Nuclear Energy

INL/RPT-25-82868

Leveraging MARVEL And SPHERE To Demonstrate NEAMS Thermal Hydraulics Codes

Joshua E. Hansel,
Vasileios Kyriakopoulos, and
Lise Charlot
Idaho National Laboratory

December 2024

Idaho National Laboratory
Computational Frameworks
Idaho Falls, Idaho 83415

http://www.inl.gov

Prepared for the
U.S. Department of Energy
Office of Nuclear Energy
Under DOE Idaho Operations Office
Contract DE-AC07-05ID14517

Page intentionally left blank

ABSTRACT

Single Primary Heat Extraction and Removal Emulator (SPHERE) and Microreactor Applications Research Validation and Evaluation (MARVEL) were utilized to demonstrate thermal hydraulics codes of the Nuclear Energy Advanced Modeling and Simulation (NEAMS) program.

A recent long-duration test of a sodium heat pipe conducted at the SPHERE facility was utilized to validate the heat pipe code Sockeye. The first 10 hours of operation featured a startup of the heat pipe from room temperature; this portion was modeled with Sockeye and compared to the experimental data. Among the data were several thermocouple measurements across the length of the heat pipe surface. Two of Sockeye's heat pipe models were applied to the experiment, as well as several models of the cooling at the condenser end of the heat pipe. The Sockeye results reflected decent agreement with the experimental data, with a notable discrepancy being seen in the condenser section, where the experimental data indicated a significant inactive length of the heat pipe.

The MARVEL microreactor was modeled through a coupled simulation of System Analysis Module (SAM) and SubChannel Module (SCM). This multiscale coupled simulation was performed as an exercise to demonstrate the compatibility and applicability of these codes for microreactor thermal-hydraulic analysis. Coupling of the SCM and SAM codes for multiscale modeling of MARVEL was achieved through a domain overlapping approach. In this example, a transient SAM simulation provided boundary conditions to SCM, and SCM provided a pressure drop to SAM.

Page intentionally left blank

ACKNOWLEDGMENTS

We would like to thank Zachary Sellers and Jeremy Hartvigsen for providing data on the Single Primary Heat Extraction and Removal Emulator (SPHERE) experiment, and for the time and effort they devoted to answering questions related to the experiment and responding to feedback. We would also like to thank Jeffrey Diebold and Calin Tarau of Advanced Cooling Technologies (ACT) for lending their expertise on heat pipe operation, interpreting SPHERE data, and offering experimental advice.

This work was funded by the Office of Nuclear Energy of the U.S. Department of Energy, through the Nuclear Energy Advanced Modeling and Simulation (NEAMS) program, under contract no. DE-NE0008983. Sockeye and SubChannel Module (SCM) development are being carried out under the auspices of Idaho National Laboratory, a contractor of the U.S. Government, under contract no. DEAC07-05ID14517. Accordingly, the U.S. Government retains a nonexclusive, royalty-free license to publish or reproduce the published form of this contribution, or allows others to do so, for U.S. Government purposes.

Page intentionally left blank

CONTENTS

FIGURES

TABLES

ACRONYMS

ACT	Advanced Cooling Technologies
LCVF	liquid-conduction, vapor-flow
MARVEL	Microreactor Applications Research Validation and Evaluation
MOOSE	Multiphysics Object-Oriented Simulation Environment
NEAMS	Nuclear Energy Advanced Modeling and Simulation
PCS	primary coolant system
SAM	System Analysis Module
SCM	SubChannel Module
SPHERE	Single Primary Heat Extraction and Removal Emulator

Page intentionally left blank

Leveraging MARVEL and SPHERE to Demonstrate NEAMS Thermal Hydraulics Codes

1. INTRODUCTION

The most recent development in the nuclear industry is that reactors are getting smaller. Multiple microreactor designs are currently under development in the United States and may be ready to deploy within the next decade. These compact reactors will be small enough to be transported by truck, and could help resolve certain energy challenges in several areas, ranging from remote commercial/residential locations to military bases.

Microreactor designs vary, but most would be able to produce 1–20 MW of thermal energy directly usable as heat or convertable to electric power. They can generate clean, reliable electricity for commercial use or for non-electric applications such as district heating, water desalination, and hydrogen fuel production.

One subset of microreactors was designed to transfer heat from the reactor via heat pipes, which were selected for their compact design, passive operation, and high thermal efficiency. Heat pipes have been used for several decades in a variety of applications such as air conditioning, oil pipelines, electronics cooling, and space radiators [1, 2]; however, substantially less experience and fewer data are available for high-temperature heat pipes such as those proposed for microreactors.

The success and adoption of these microreactor designs depends on their safety characteristics and efficiency, both of which are tied to reactor core performance. It is important to demonstrate that a fuel design can operate reliably at high burnups, high power densities, and high coolant temperatures. The operational limitations involved, such as clad thermal creep, corrosion, and clad wastage formation, are all highly temperature-dependent phenomena. Consequently, accurate prediction of temperature distributions during normal operation, as well as during transients, is key to demonstrating the safety of these designs. As a result, validated tools and models are needed to evaluate the passive safety features, design, and performance of microreactors.

The Nuclear Energy Advanced Modeling and Simulation (NEAMS) program has developed several thermal hydraulics codes, including Sockeye and the SubChannel Module (SCM), both of which are based on the Multiphysics Object-Oriented Simulation Environment (MOOSE) framework. MOOSE is an open-source, finite element framework upon which a variety of physics applications are built, including several that are highly relevant to microreactors [3, 4]. Most notable in this regard is DireWolf, a multiphysics code that couples neutronics, thermomechanics, and thermal hydraulics (see, for example, [5]).

One of the codes included in DireWolf is Sockeye, which models high-temperature heat pipes often used in microreactors. Heat pipes feature geometrically complex, porous wick structures, making it computationally intractable to generate a mesh of their interiors. The potential computational complexity is exacerbated by the need to use models of compressible and two-phase flows. Since it would be prohibitively expensive to use a high-fidelity model of each of the several hundred heat pipes in a microreactor core, Sockeye is designed for the engineering scale, employing 1D and 2D models. Sockeye offers three heat pipe models: a 1D, two-phase compressible flow model [6]; a 2D heat conduction model [7]; and the liquid-conduction, vapor-flow (LCVF) model, which is a 1D, single-phase compressible flow model for the vapor phase, coupled to a 2D heat conduction model for the liquid phase [8].

While heat pipes have been used for several decades, the experience and data on high-temperature heat pipes such as those proposed for microreactors are insufficient for design and analysis. The Single Primary Heat Extraction and Removal Emulator (SPHERE) facility at Idaho National Laboratory was designed to enable non-nuclear thermal and integrated systems testing of heat pipes under a range of operating

conditions [9]. Several sodium heat pipe experiments have been performed at SPHERE in the time since its inception, some of which have been utilized for Sockeye validation purposes [7]. Recently, a long-duration experiment was performed [10], and the present work utilizes this experiment for the validation of Sockeye.

The Microreactor Applications Research Validation and Evaluation (MARVEL) is a 85 kWth, thermal spectrum, sodium-potassium eutectic (NaK)-cooled microreactor developed under the leadership of Idaho National Laboratory via the U.S. Department of Energy's Microreactor Program [11]. This microreactor, once operational, can be used by researchers and technology developers to gain operational experience and advance the technical maturity of microreactor concepts. It is designed to use Training, Research, Isotopes, General Atomics (TRIGA) international fuel (20% enriched) and operate at high enough temperatures to serve as a heat source for power production via Stirling engines and/or high-grade heat for microgrid applications. MARVEL's primary coolant system (PCS) is a 4-loop hydraulic circuit, assembled to efficiently transport nuclear fission heat from the nuclear fuel to the heat addition section of the secondary coolant system by utilizing natural circulation of liquid NaK, while also maintaining the reactor fuel at a suitable operating temperature. The PCS also transfers decay and sensible heat to the ultimate heat sink, the reactor cavity pit, via heat conduction and convection following any reactor shutdown.

Measurements collected from the operation of the MARVEL reactor can also be leveraged for the validation of NEAMS tools. A multiphysics model is currently under development [12]. The primary and secondary loops have been modeled using the System Analysis Module (SAM) [13], and preliminary results showed some radial and azimuthal variations in the pin power profiles. Thus, a higher-fidelity approach than the 1D one is desirable for improving the accuracy of the results. Subchannel codes are thermal-hydraulic codes that offer an efficient compromise between computational fluid dynamics codes and system codes when simulating a nuclear reactor core. They use a quasi-3D model formulation as well as a subchannel discretization that allows for a finer mesh than system codes, without entailing the high computational costs of computational fluid dynamics. Integration of the conservation equations (momentum, energy, mass) over these volumes will produce the subchannel equations. Various subchannel codes have been developed or adapted to liquid-metal reactor designs.

SCM, the MOOSE [3] module for subchannel analysis [14], was developed to model single-phase flows through liquid-metal-cooled, wire-wrapped fuel pin sub-assemblies ordered in a triangular lattice [15, 16]. This makes SCM an ideal candidate for modeling the thermal hydraulics phenomena in the MARVEL core. However, it is only applicable to the core region, and modeling the loop feedback in MARVEL is important because the flow is driven by natural convection. This can be addressed by coupling a core model that uses SCM to a loop model that uses SAM.

This paper is outlined as follows. Section 2 discusses utilization of the SPHERE long-duration experiments for the validation of Sockeye, Section 3 summarizes the coupled SAM-SCM model of MARVEL, and Section 4 offers conclusions stemming from this work.

2. SOCKEYE VALIDATION USING SPHERE

2.1. SPHERE Experimental Setup

This section describes the setup of SPHERE for its most recent experiments [10]. Figure 1 shows a photo of the assembly, exterior to the stainless-steel sanitary tube, which contains the heater, heat pipe, calorimeter, and insulation. The parameters of the sanitary tube are given in Table 1. The thermal properties were computed from temperature-dependent correlations of stainless steel. The sanitary tube is composed of five sections. These roughly correspond to the following list, starting at the condenser end (i.e., the left end in Figure 1):

1. Calorimeter fluid lines

2. Condenser section
3. Adiabatic section
4. Evaporator section
5. Instrumentation leads.

The inner surface of the chamber is covered by a zirconia ceramic-fiber insulation blanket. The outer surface of the middle three sections of the chamber is insulated by a thin layer of Nomex aramid insulation in order to protect personnel from contact burns. A vacuum established in the sanitary tube eliminates convective heat transfer, so solid regions separated by gaps transfer heat via radiation only.

Table 1. Sanitary tube parameters.

Parameter	Value
Material	Stainless steel
Emissivity	0.7
Outer diameter	12 in.
Thickness	0.134 in.

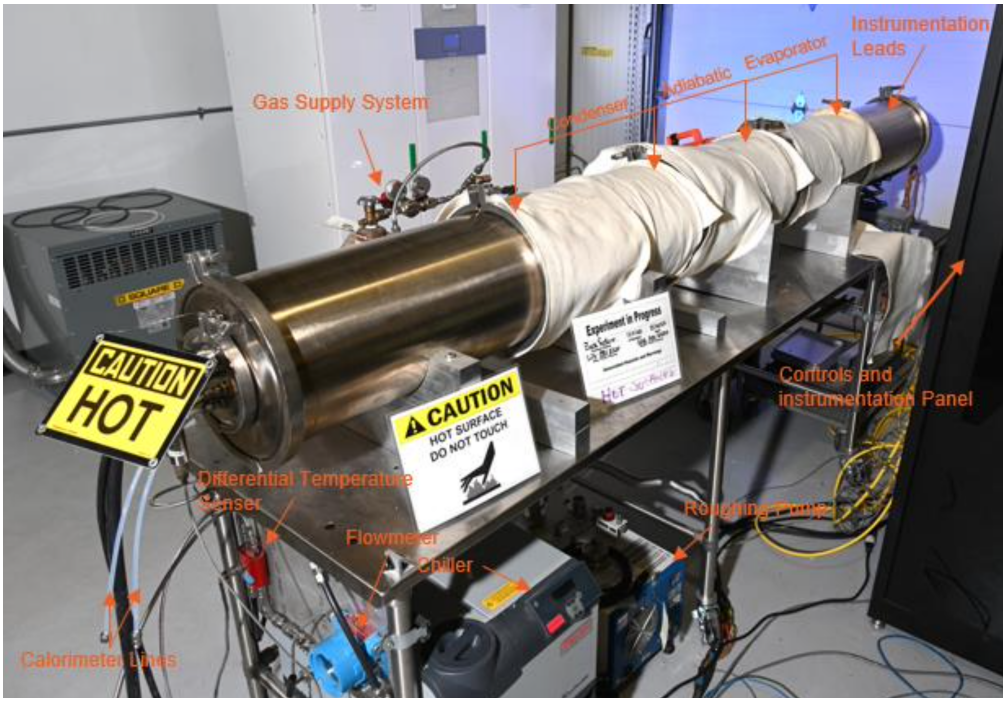

Figure 1. SPHERE setup.

Thermocouples are mounted via wire ties to the heat pipe surface at various axial positions. A fan blows air over the sanitary tube section containing the instrumentation leads, the intent being to prevent overheating of the instrumentation leads, as the feedthrough wire that exits the sanitary tube is limited to 80°C.

The heating assembly is comprised of two semi-cylindrical ceramic-fiber heaters manufactured by Watlow [17]. One of these is shown in Figure 2. The black surface corresponds to a high-emissivity coating. The geometrical and material parameters of the heater are given in Table 2.

Figure 2. Half the SPHERE heater assembly.

The adiabatic section of the heat pipe is covered with a ceramic fiber insulation blanket from CeraMaterials, the parameters of which are given in Table 3. The thermal conductivity is linearly interpolated/extrapolated from the given points.

The calorimeter, shown in Figure 3, is comprised of a stainless-steel coil surrounded by a stainless-steel shroud, the parameters of which are given in Table 4. The thermal properties were computed from temperature-dependent correlations of stainless steel. Water at an inlet temperature of approximately 20°C enters the coil from the condenser end and flows toward the adiabatic section. The difference in temperature ΔT is measured, as is the water mass flow rate $\dot{m}$, allowing for the calorimeter heat removal rate $\dot{Q}_{\text{cal}}(t)$ to be computed as follows:

$$\dot{Q}_{\text{cal}}(t) = \dot{m}(t) c_p \Delta T(t)\,, \tag{1}$$

where c_p is the specific heat capacity of water under these conditions.

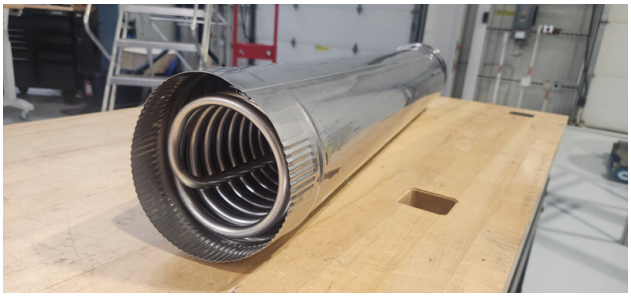

Figure 3. SPHERE calorimeter.

The sodium heat pipe was manufactured by Advanced Cooling Technologies (ACT). Its internal specifications are proprietary and thus not listed in this report. The heat pipe was not designed with non-condensable gases; however, models were run both with and without an assumed mass of 0.5 mg of air

Table 2. Heater parameters.

Parameter	Value
Material	Alumina-silica ceramic fiber
Density	200 kg/m^3
Specific heat capacity	1000 J/(kg-K)
Thermal conductivity	0.15 W/(m-K)
Heated surface emissivity	0.9
Unheated surface emissivity	0.7
Total length	30 in.
Heated length	24 in.
Heat pipe heated length	22 in.
Inner diameter	6.5 in.
Outer diameter	10.5 in.
Heated thickness (estimated)	0.5 in.

Table 3. Adiabatic section insulation parameters.

Parameter	Value
Material	Zirconia ceramic fiber
Density	8 lb/ft^3
Specific heat capacity	1246 J/(kg-K)
Thermal conductivity	0.176 W/(m-K) at 800°C 0.22 W/(m-K) at 1000°C
Emissivity	0.7
Length	23.75 in.
Thickness	1 in.

in order to investigate possible discrepancies with the measured data.

The experiment began at room temperature (approximately 20°C), with the sodium working fluid in the heat pipe being frozen. The power to the heater was gradually increased, in steps, over the course of several hours, eventually reaching roughly 1500 W at around 7.5 hours into the experiment. The calorimeter pump was turned on roughly 5.5 hours into the experiment. Up until that point, its fluid (water) was stationary in the coil tubes.

Table 4. Condenser section parameters.

Parameter	Value
Coil tube material	Stainless steel
Shroud material	Stainless steel
Emissivity	0.7
Length	30 in.
Coil tube outer diameter	0.375 in.
Coil tube wall thickness (assumed)	1 mm
Shroud outer diameter	6 in.

2.2. SPHERE Model Description

The SPHERE assembly was approximated using the geometry shown in Figure 4, which also shows the axial locations of each thermocouple. Note that because the thermocouple located at the 51.5” position was believed to have fallen off the heat pipe and was thus measuring the temperature of the bottom of the vessel, it is omitted from the results.

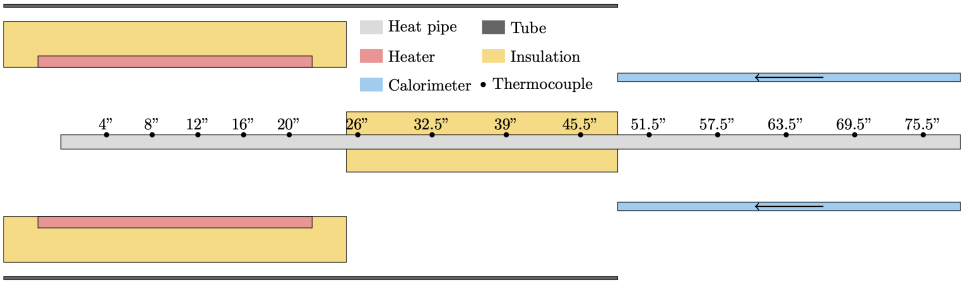

Figure 4. SPHERE model geometry diagram.

The experiment was approximated as a 2D axisymmetric problem, since the setup is relatively azimuthally uniform despite there being notable azimuthal dependencies such as the structural supports that suspend the components along the axis of the sanitary tube.

The heater was modeled using a 2D heat structure, with a uniform volumetric heat source in the heated region of the heater assembly. The actual heater coils were embedded within the ceramic fiber, and were approximated to reside within a region possessing a thickness of 0.5 in., starting at the inner surface, as shown in Figure 4. The adiabatic section insulation was also modeled using a 2D heat structure.

The calorimeter geometry was made complex by the coiled fluid line; therefore, the geometry was simplified to consist of a cylindrical shell sharing the same axis as the heat pipe, with the coolant fluid flowing in an annular cross section around the shell. The thickness of this annular channel was taken to be the inner diameter of the coil tube so as to give approximately the same total volume.

Radiative heat transfer was used to couple the various surfaces separated by a gap. The surfaces were assumed to be opaque, gray, and diffuse, and an infinite length approximation was applied, causing the surface elements to only be coupled to their radial neighbors at the same axial position. The resulting heat flux to surface i, q_i was computed as follows:

$$q_i(x,t) = \frac{\sigma \left[T_j(x,t)^4 - T_i(x,t)^4\right]}{\mathcal{R}_i}, \tag{2}$$

where σ is the Stefan-Boltzmann constant and T_i is the temperature of surface i. $\mathcal{R}_i$ is the radiation resistance:

$$\mathcal{R}_i = \frac{1-\epsilon_i}{\epsilon_i} + \frac{1}{F_{i,j}} + \frac{1-\epsilon_j}{\epsilon_j}\frac{A_i}{A_j}\,, \tag{3}$$

where ϵ_i is the emissivity of surface i, $F_{i,j}$ is the view factor from surface i to surface j, and A_i is the area of surface i. For a two-surface enclosure, the enclosed surface i has a view factor of unity ($F_{i,j} = 1$). The other surface view factor $F_{j,i}$ may then be computed using the reciprocity rule.

The sanitary tube walls were included along the length of the heater block and the adiabatic section, but not along the length of the condenser section, where all heat leaving the heat pipe surface was assumed to enter the calorimeter wall.

Radiation boundary conditions were applied to the outer surface of the sanitary tube. Equation (2) reduces to:

$$q(x,t) = \sigma\epsilon\left[T_\infty^4 - T(x,t)^4\right]\,, \tag{4}$$

where T_∞ is the environmental temperature, assumed to be 20°C.

Several cooling models were considered in applying cooling to the outer surface of the wall between the gap and the calorimeter fluid (water):

- **Flux**: The experimentally measured calorimeter power $\dot{Q}_{\text{cal}}(t)$ was used directly:

$$q(t) = \frac{\dot{Q}_{\text{cal}}(t)}{\pi D_{\text{wall}} L_{\text{cond}}}\,, \tag{5}$$

  where D_{wall} is the outer diameter of the calorimeter wall and L_{cond} is the length of the condenser.
- **Specified heat transfer coefficient**: The following convection boundary condition was applied:

$$q(x,t) = h(T_{\text{fluid}} - T_{\text{wall}}(x,t))\,, \tag{6}$$

  where the fluid temperature T_{fluid} is considered constant at the inlet temperature:

$$T_{\text{fluid}} = T_{\text{inlet}}\,, \tag{7}$$

  and the heat transfer coefficient is specified directly via the function $h(t) = f(t)$. With the geometry simplification, the use of realistic correlations for heat transfer coefficients was no longer beneficial, as the flow speed, direction, and cross section no longer applied. Therefore, we selected a heat transfer coefficient—namely, 35 W/(m^2-K)—that produced a reasonable match with the experimental data.
- **Controlled heat transfer coefficient**: As with the "Specified heat transfer coefficient" cooling model, the fluid temperature was considered constant at the inlet temperature. However, the heat transfer coefficient was dynamically adapted to produce the measured calorimeter power.
- **Flow**: The coolant fluid was modeled with a 1D flow channel, as well as with convection coupling:

$$q(x,t) = h(T_{\text{fluid}}(x,t) - T_{\text{wall}}(x,t))\,. \tag{8}$$

  The mass flow rate at the channel inlet was set to be the experimentally measured mass flow rate ($\dot{m}(x_{\text{in}},t) = \dot{m}_{\text{exp}}(t)$), and the channel outlet was set to have a pressure of 100 kPa. As with the "Specified heat transfer coefficient" cooling model, the heat transfer coefficient was chosen so as to give a reasonable match with the experimental data. To enable useful comparison, the same value was used. The outer surface of the annular flow channel was approximated as being perfectly insulated.

The heat pipe was modeled using two of Sockeye's heat pipe models:

- **LCVF Model**: The vapor phase of the working fluid was modeled with 1D compressible flow, and the liquid-filled wick and cladding were modeled with 2D heat conduction [8].
- **Conduction Model**: The entire heat pipe was modeled using 2D heat conduction. An effective thermal conductivity value was used for the vapor core of the heat pipe, which mimicked the real performance of the heat pipe, based on analytic operating limit relations evaluated at the current temperature [7].

2.3. SPHERE Results

In this section we present the results of the various models described in Section 2.2. The first 10 hours of the experiment were modeled, as this is the most interesting portion of the 1,000-hour experiment.

The 1D vapor flow channel in the LCVF model was discretized in space via the finite volume method, and all 2D heat conduction regions were discretized via the Galerkin finite element method. Table 5 gives the numbers of axial elements in each length. All 2D regions are modeled with three radial elements in each region. The BDF-2 scheme, which is second-order accurate, fully implicit, and A-stable, was used to discretize in time, and an adaptive time step size was employed that sought out the time step size such that the nonlinear solve converged in a given number of iterations, with the maximum time step size being 150 s.

Table 5. Numbers of axial elements.

Length Name	Number of Elements
Heater block unheated length (each)	3
Heated length overlapping with heat pipe	22
Heated length not overlapping with heat pipe	2
Adiabatic section	24
Condenser section	30

First, we consider the LCVF model that features the simplest cooling model, which uses a uniform heat flux set to the experimentally measured heat removal rate. The results, shown in Figure 5, are predictably poor. The uniform heat removal approximation causes the temperatures in the inactive region to plummet to unphysical values and cause failure of the solution, as very little heat is able to get to these points and the heat flux condition has none of the temperature feedback a convection condition would have. These results clearly indicate that, if there is indeed an inactive length in the heat pipe, the heat distribution along the condenser length is non-uniform in reality. This motivates the use of a non-uniform, temperature-dependent cooling model.

Next, instead of applying a uniform heat flux, we applied the "Controlled heat transfer coefficient" cooling model. The temperature transient is shown in Figure 6. Since the convection condition cannot result in cooling below the lowest temperature (i.e., the calorimeter inlet temperature T_{inlet}), the temperatures do not drop to unphysical values. The first several hours of the experiment (which are not cooled by the calorimeter) match up fairly well, especially the temperatures in the evaporator and adiabatic sections. In the experiment, condenser temperatures started to rise after 2 hours, but not as sharply as the temperatures in the other sections. The Sockeye condenser temperatures also began to increase, but at a much smaller rate. The temperature dips at the onset of the calorimeter operation (shortly after 5.5 hours) are visible in both the data and the Sockeye results, but are much more apparent in the Sockeye results, due to the discrepancy between the experimentally estimated power removal via the temperature difference and the heat rate from the calorimeter wall. The outlet temperature measurement was actually taken several inches downstream of the coupled section, so during the startup portion, the stationary water was being heated, with no effect on the experimentally measured heat removal rate. The calorimeter was then turned on, and suddenly all the hot water exited at once, resulting in a large-magnitude spike in the reported calorimeter power. Upon recovery from the calorimeter onset, power increases eventually caused the Sockeye temperatures to climb and converge toward each other, suggesting that the net losses in the Sockeye simulation (which include both losses to the environment and the calorimeter power) are too small. This may be due to inaccurate heat transfer boundary conditions in the evaporator and adiabatic sections, and/or perhaps to neglecting other losses in the condenser section that do not get captured by the calorimeter.

The various powers and heat rates are shown in Figure 7. The sets are described as follows:

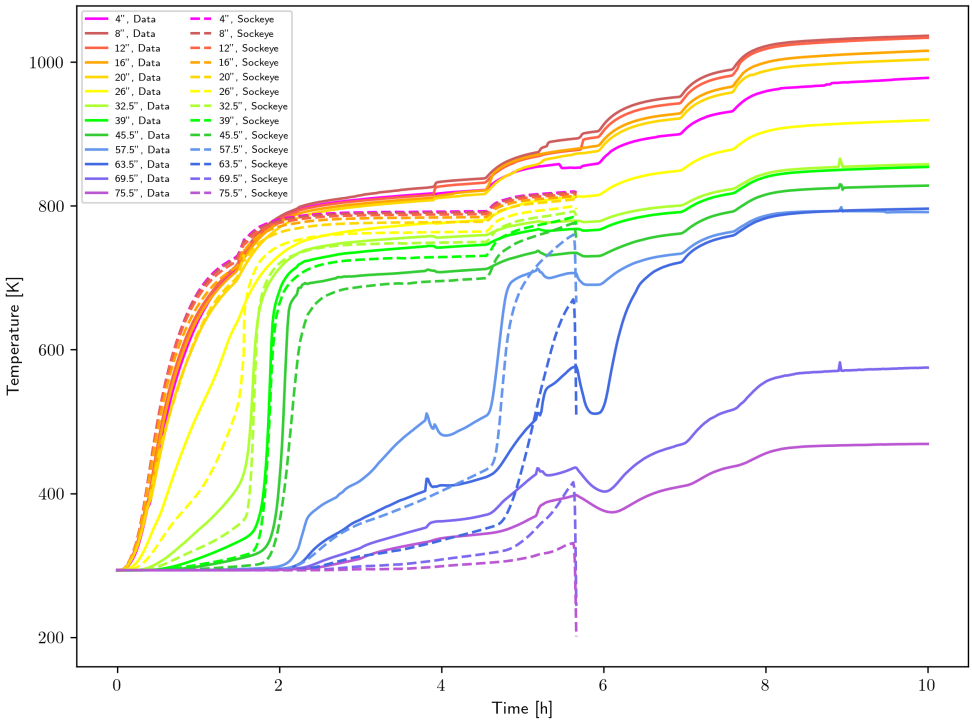

Figure 5. Temperature transient comparison between Sockeye and the experimental data for the LCVF heat pipe model that featured the uniform heat flux cooling model with non-condensable gas added.

- "Heater, Data": The heater input electrical power.
- "Cooler, Data": The experimental calorimeter power estimated via Equation (1).
- "Sonic Limit": The sonic operational heat pipe limit, estimated via an analytic relation at the current evaporator end vapor temperature in Sockeye.
- "Capillary Limit": The capillary operational heat pipe limit, estimated via an analytic relation at the current evaporator end vapor temperature in Sockeye.
- "Heater, Sockeye": The heater input power that is applied in Sockeye and which is interpolated from the experimental data.
- "HP Heat Rate, Sockeye": The heat rate across the evaporator-adiabatic interface in the vapor core in the heat pipe, which is used in comparison against to the analytic limits in Sockeye.
- "Evap. Radial Loss, Sockeye": The heat loss rate through the outer system boundaries in the evaporator section in Sockeye.
- "Evap. End Loss, Sockeye": The heat loss rate through the axial, evaporator end of the heating block in Sockeye.
- "Adia. Loss, Sockeye": The heat loss rate through the outer system boundaries in the adiabatic section in Sockeye.
- "Cooler, Sockeye": The heat loss rate through the calorimeter section in Sockeye.
- "Total Losses, Sockeye": The sum of all heat losses in Sockeye. At steady state, this should match "Heater, Sockeye."

By comparing "HP Heat Rate, Sockeye" to the limit curves, it was predicted that the heat pipe would only be limited during the first hour of the experiment. Roughly 60% of the heater power is lost through the evaporator boundary. Much less is lost through the adiabatic section boundary.

At this point, we must note that the evaporator thermocouples were believed to carry a significant amount

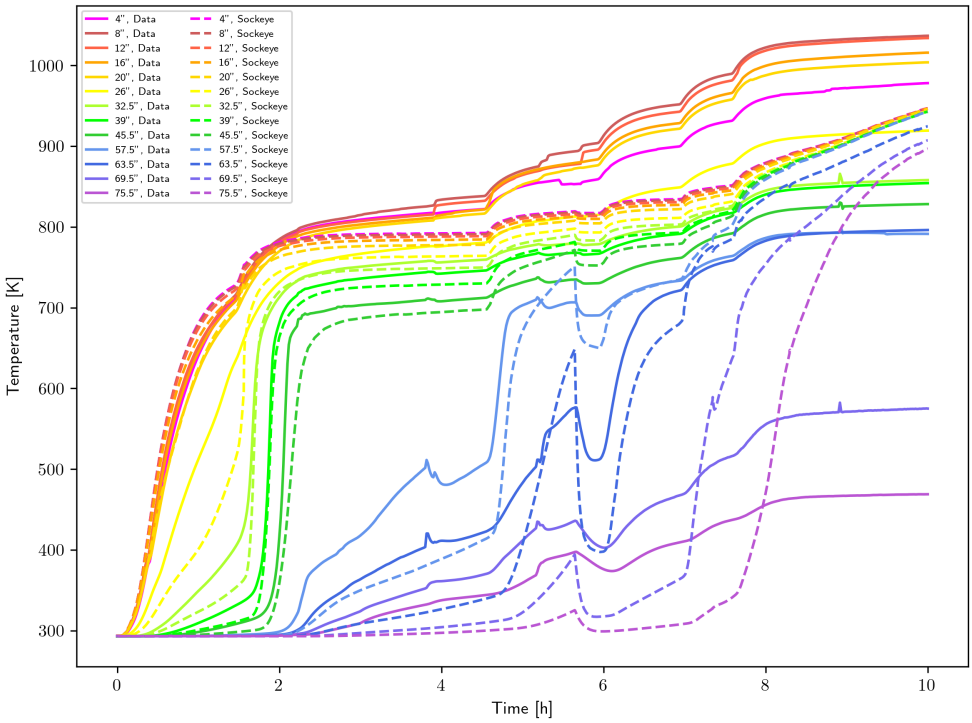

Figure 6. Temperature transient comparison between Sockeye and the experimental data for the LCVF heat pipe model featuring the controlled heat transfer coefficient cooling model with non-condensable gas added.

of error. Upon observing the significant temperature differences between the evaporator and adiabatic section, issues were suspected, as isothermal performance had been achieved at lower operating temperatures by ACT. After some discussion with ACT, the cause was believed to be the fact that the thermocouples were wire-tied to the heat pipe instead of tack-welded. It was noted that wire-tying can introduce a significant amount of thermal resistance. Additionally, with the thermocouples being directly heated by radiation, they can read much higher. Similar arguments can be made for temperatures being measured too low in the cooled sections. The adiabatic section is potentially the most trustworthy region, as little heat loss should occur there.

Since it was found that directly applying the experimentally estimated calorimeter power for the cooling condition led to underestimation of losses, the next approach was the "Specified heat transfer coefficient" cooling method, in which it was accepted that error existed in the cooling approximation and that an artificial, larger heat transfer coefficient may be more appropriate. Per trial and error, the value $h = 35$ W/(m^2-K) was found to match up with the data decently well. The results are shown in Figure 8. The condenser temperatures have a very delayed rise, but the final temperatures do not falsely converge to each other as they do in Figure 6.

Finally, the "Flow" cooling model was applied. This is the most mechanistic of the options, and offers an advantage over the "Specified heat transfer coefficient" cooling model in that the coolant fluid temperature can now vary from the inlet temperature. The results are shown in Figure 9. Since the calorimeter fluid was not fixed at the inlet temperature, the condenser section temperatures could increase much earlier and end up at hotter values. As this is considered the best set of models applied to this experiment, we examined some additional plots to understand what was happening in the system. The final temperature distribution is shown in Figure 10. The experimental data reflect a noticeable peak in the evaporator section, but for the time being we assumed this to largely stem from measurement error. The adiabatic and condenser sections saw decent, though still not excellent, matches between the data and the Sockeye results. The vertical line "Inactive start" denotes the start of the inactive length of the heat pipe, which is composed of two components: the excess

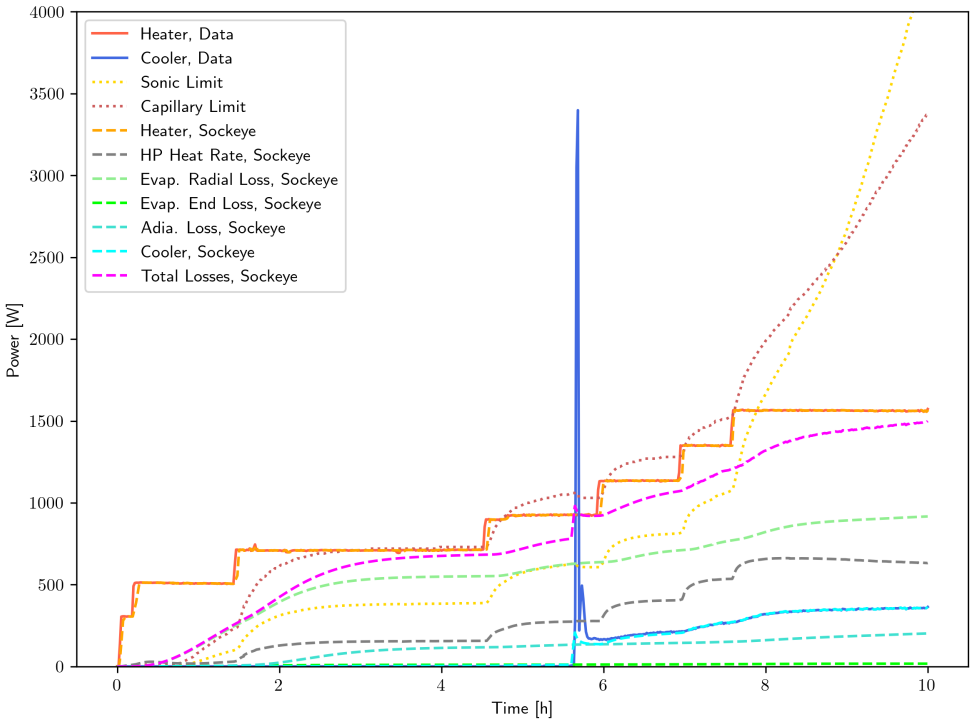

Figure 7. Power transient comparison between Sockeye and the experimental data for the LCVF heat pipe model featuring the controlled heat transfer coefficient cooling model with non-condensable gas added.

working fluid pool and the non-condensable gas pool. Figure 11 shows each of the inactive lengths as a function of time. The "Unstarted" curve corresponds to a startup front model in the LCVF model, which marks the transition between rarefied gas flow and continuum flow. This was mainly active for the first hour, after which it simply followed the "Condenser pool plus NCG" curve. The non-condensable gas pool started out very large, when the partial pressure of the working fluid was small, but shrunk significantly with increasing temperature and system pressure. The condenser pool length was roughly a few inches, and grew as the system continued to heat up due to thermal expansion of the working fluid.

The power transient is shown in Figure 12. In contrast to Figure 7, the cooling power in Sockeye is quite larger with the specified heat transfer coefficient. Also note that this approach can capture some of the peak associated with the onset of calorimeter flow.

In an effort to investigate the possibility of the sonic limit being active and causing the significant temperature differences across the heat pipe, we present, in Figure 13, the final time vapor Mach number profile. The Mach number reaches a peak of 0.16 at the evaporator section exit, indicating that—at least at the final time—the heat pipe is not under the sonic limitation. The "Inactive start" line denotes the location of the dynamic wall boundary condition that is imposed in the LCVF model, which is designed to mimic the working fluid's inability to reach the end of the heat pipe, due to the effects of the non-condensable gases and excess working fluid.

Next, the effect of the choice of heat pipe model was investigated. The Conduction model was used with the same conditions and cooling model as represented in Figure 9. The results are shown in Figure 14. Several observations can be made. First, a small peak in the heated length temperatures occurs shortly after 1 hour. This overshoot corresponds to separation from the viscous and sonic limitations, with the thermal conductivity quickly climbing to its maximum value. Next, in comparison to the LCVF model, we observe that the temperatures have a much greater spread between 2 and 8 hours. The flow model is much better able

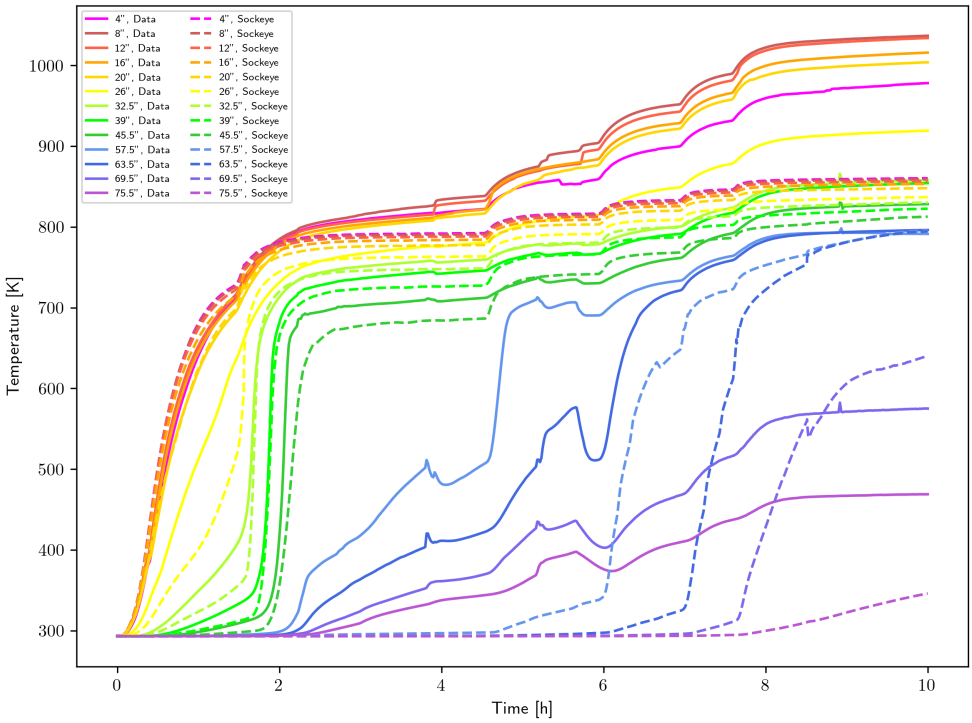

Figure 8. Temperature transient comparison between Sockeye and the experimental data for the LCVF heat pipe model featuring the specified heat transfer coefficient cooling model with non-condensable gas added.

to capture the discontinuous nature of startup. Lastly, we observe many oscillations in the 69.5” position temperature at between 6 and 8 hours. This is due to the non-condensable gas model for the Conduction model, which features a dynamic non-condensable gas front based on partial pressures. As the temperature increases, the non-condensable gas length at the end of the condenser decreases, causing more of the condenser length to be active and in turn cooling the fluid, thus increasing the non-condensable gas length. Since the Conduction model uses a very high thermal conductivity on one side of this interface and a very low thermal conductivity on the other, it can be difficult to achieve a stable interface numerically. However, note that this effect decreases as the mesh is refined. In comparing the steady-state temperature distributions of the Conduction model and LCVF model, we observe that the Conduction model has a fairly similar distribution, except for the temperatures in the inactive region of the condenser. Note that the Conduction model currently does not account for the excess working fluid in the heat pipe, so therefore the inactive condenser pool length effect is absent—likely a significant factor in causing a discrepancy.

To study the effect of non-condensable gases on the solution, we compared the results in Figures 9 and 10 against a simulation in which non-condensable gases were omitted. These results are shown in Figures 15 and 16, respectively. The startup results are similar, but post-startup, without non-condensable gases, the two temperatures at the condenser end are much higher, and the temperature gradient in the heated and adiabatic lengths is greater.

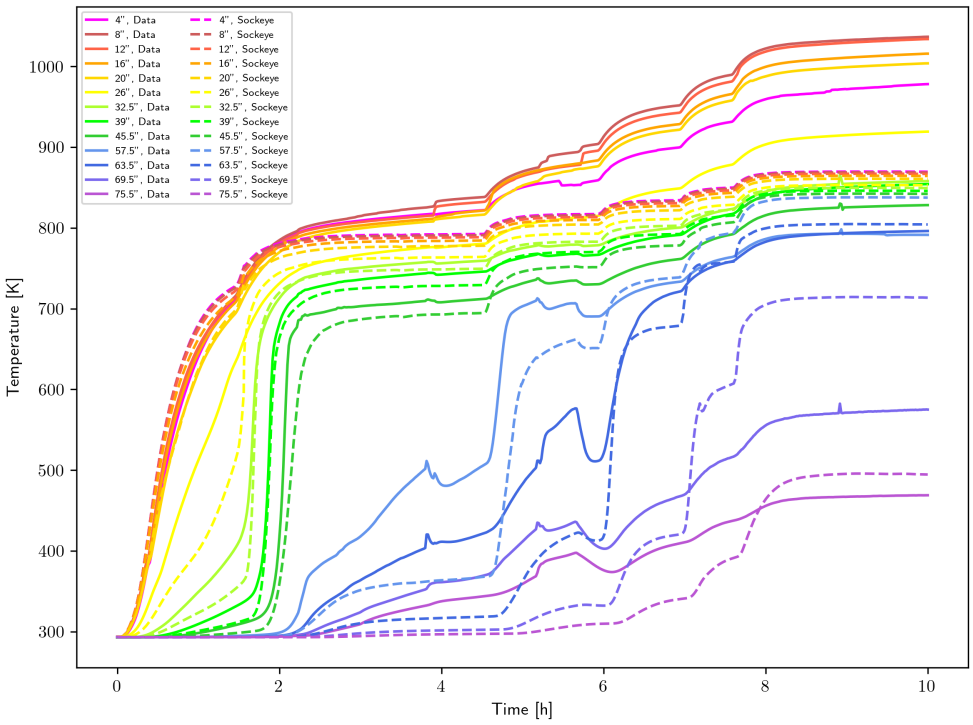

Figure 9. Temperature transient comparison between Sockeye and the experimental data for the LCVF heat pipe model featuring the flow cooling model with non-condensable gas added.

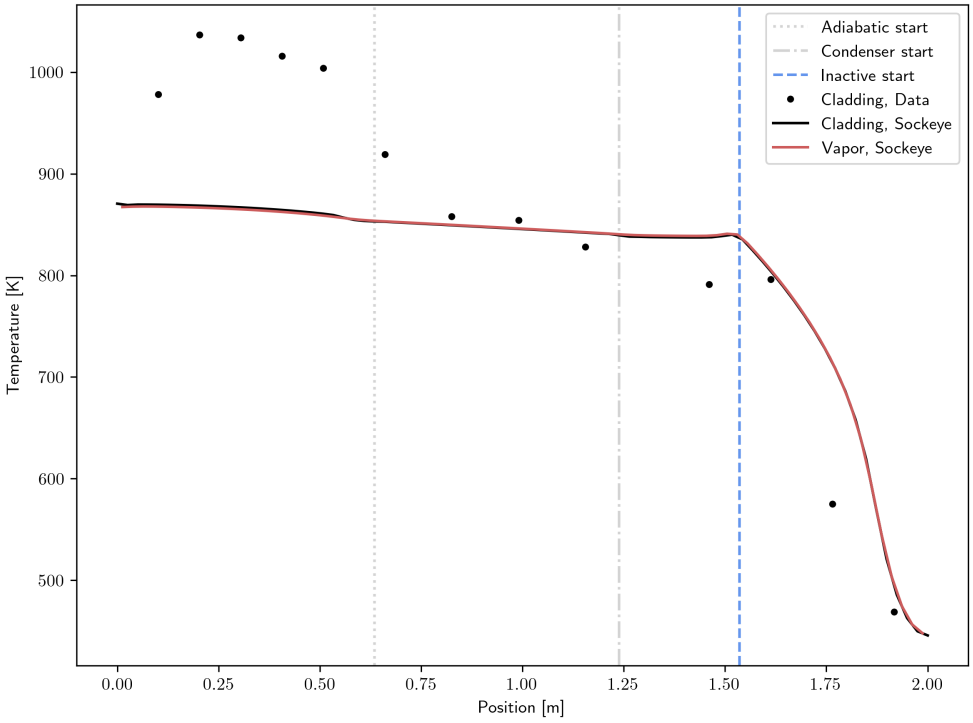

Figure 10. Final temperature profile comparison between Sockeye and the experimental data for the LCVF heat pipe model featuring the flow cooling model with non-condensable gas added.

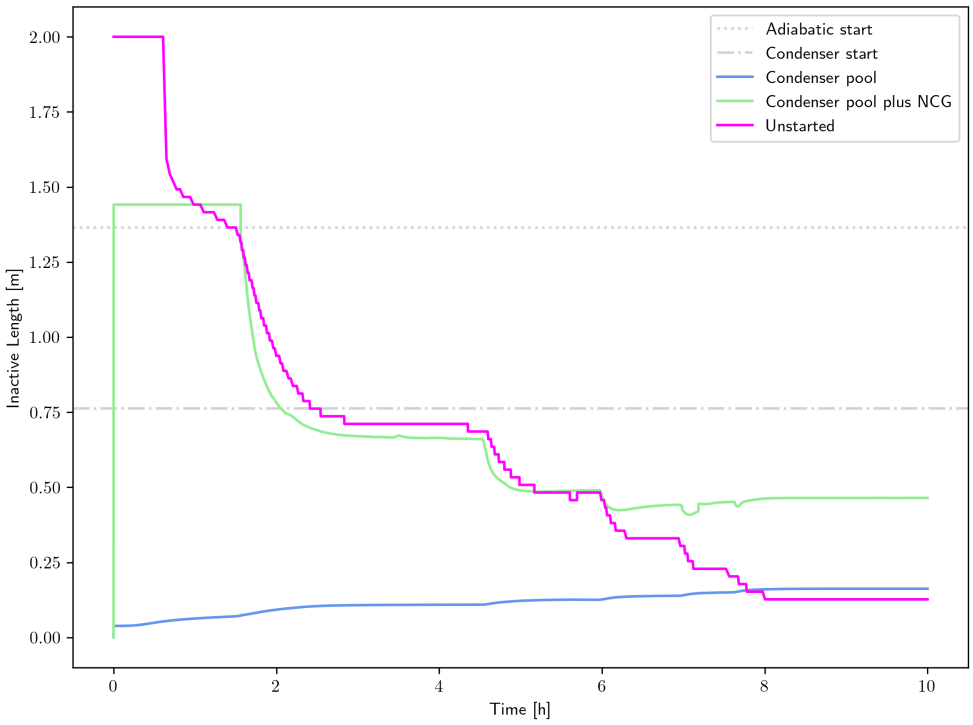

Figure 11. Inactive-length transient comparison between Sockeye and the experimental data for the LCVF heat pipe model featuring the flow cooling model with non-condensable gas added.

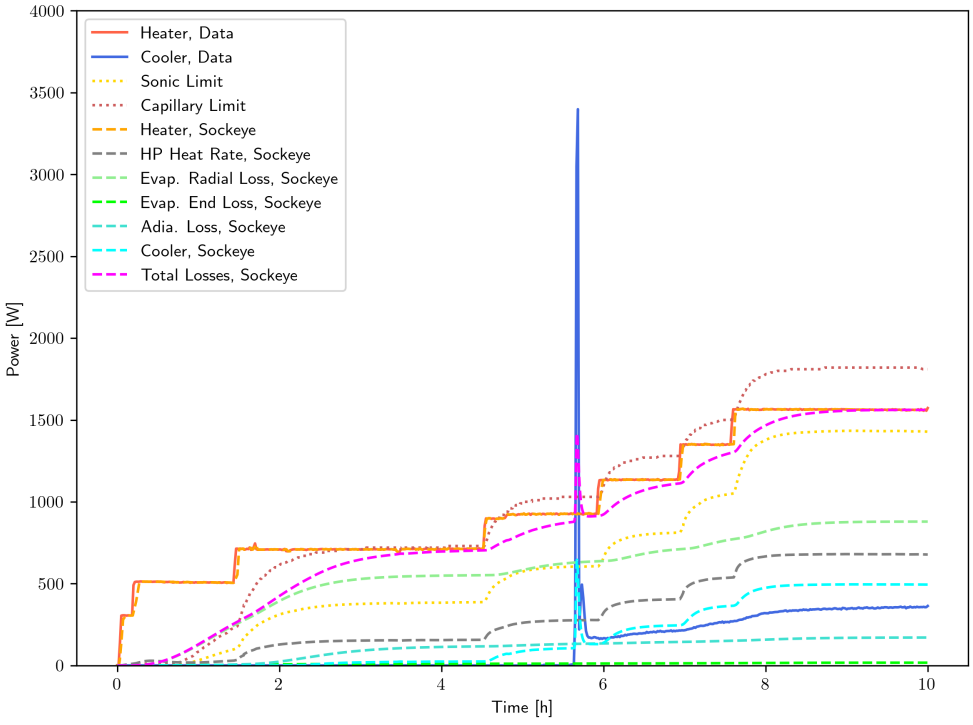

Figure 12. Power transient comparison between Sockeye and the experimental data for the LCVF heat pipe model featuring the flow cooling model with non-condensable gas added.

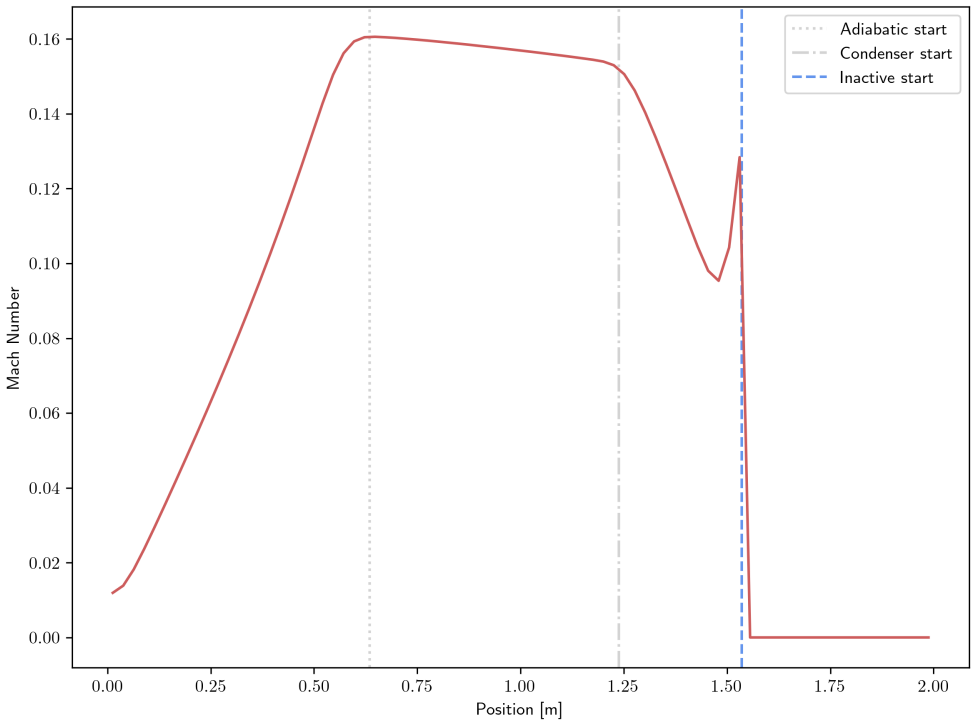

Figure 13. Final Mach number profile comparison between Sockeye and the experimental data for the LCVF heat pipe model featuring the flow cooling model with non-condensable gas added.

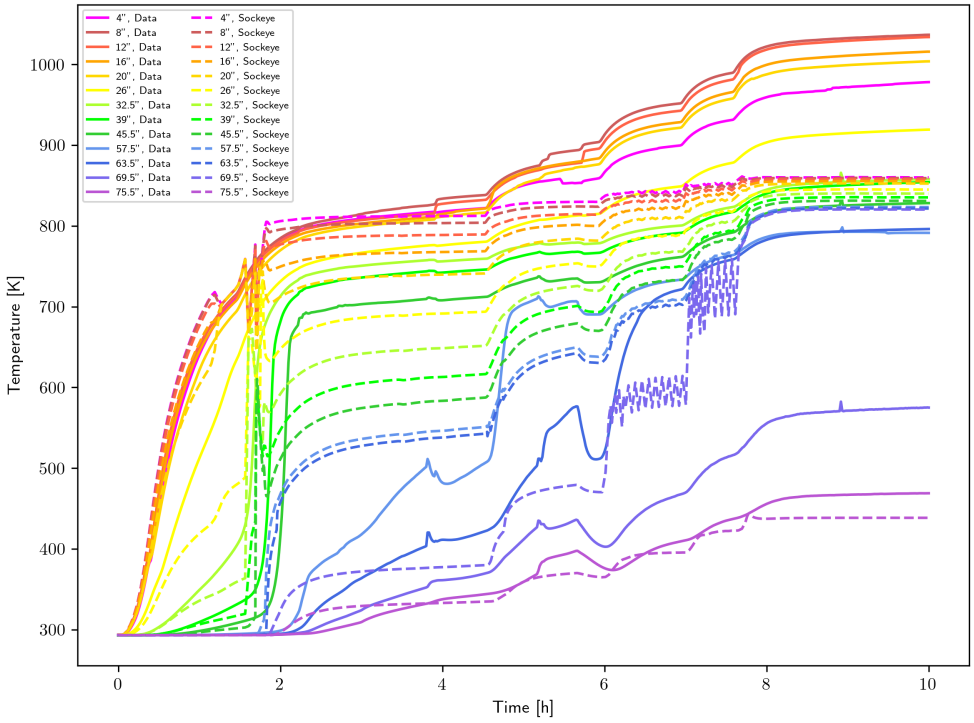

Figure 14. Temperature transient comparison between Sockeye and the experimental data for the Conduction heat pipe model featuring the flow cooling model with non-condensable gas added.

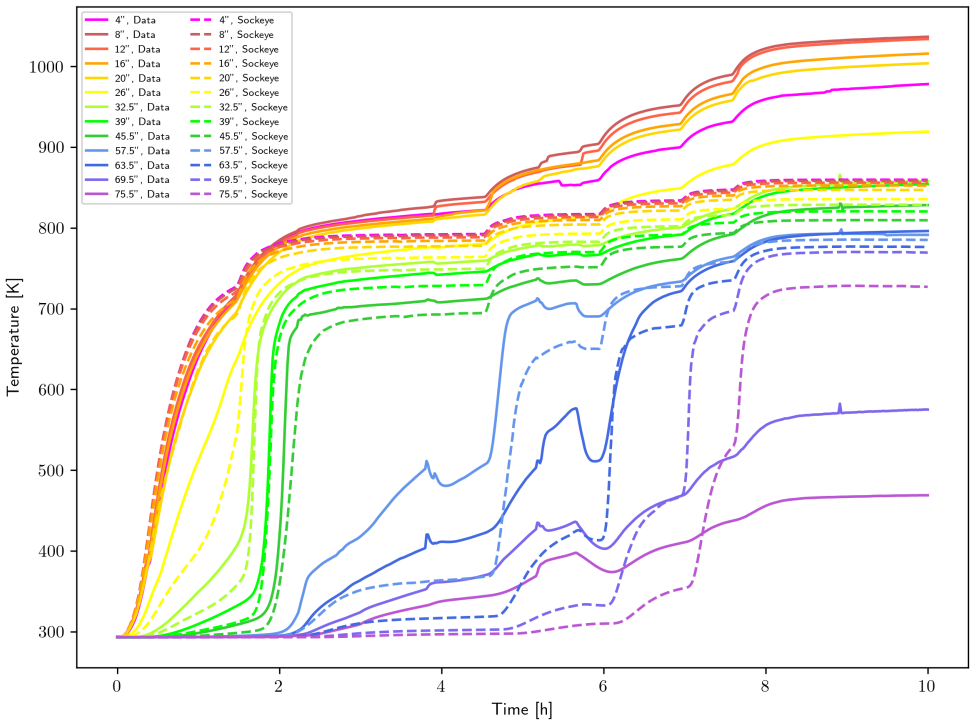

Figure 15. Temperature transient comparison between Sockeye and the experimental data for the LCVF heat pipe model featuring the flow cooling model without non-condensable gas added.

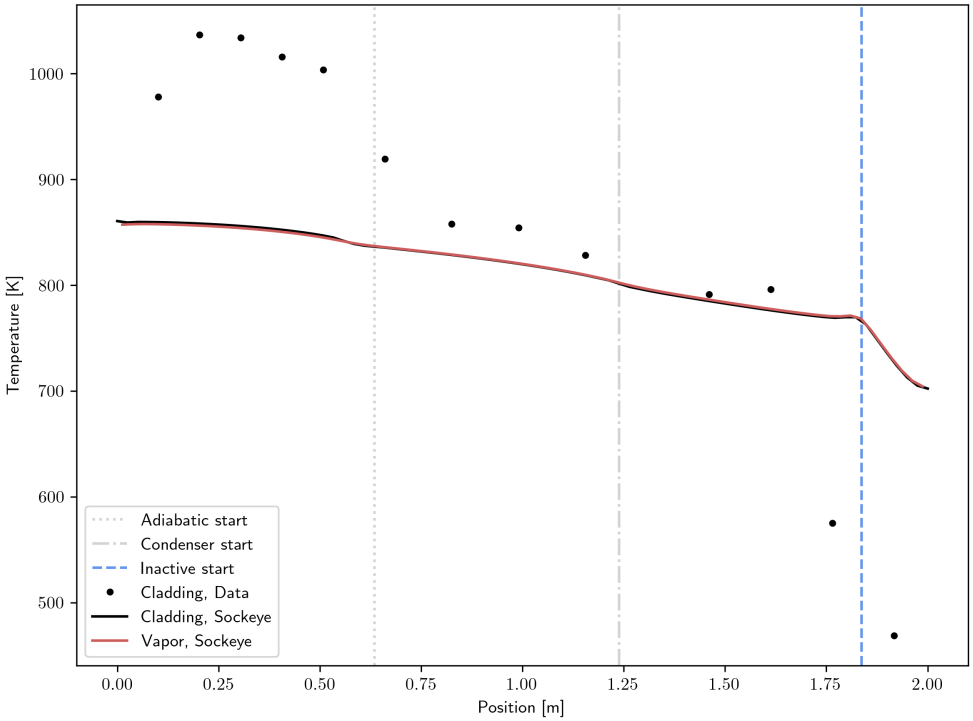

Figure 16. Final temperature profile comparison between Sockeye and the experimental data for the LCVF heat pipe model featuring the flow cooling model without non-condensable gas added.

3. SCM-SAM COUPLED SIMULATION OF A MARVEL MICROREACTOR

MARVEL is a natural-convection-cooled, sodium-potassium microreactor anticipated to generate 85 kW of thermal energy. It will operate within Idaho National Laboratory's Transient Reactor Test Facility and is being developed by the U.S. Department of Energy's Microreactor Program. MARVEL will be used to test microreactor applications, generate operational data, and pave the way for commercial demonstrations.

A thermal-hydraulic computational model of MARVEL is a valuable tool for studying important transients and calculating the safety limits of microreactor designs. For this purpose, a multiscale coupled simulation was developed: SCM is used for a subchannel model of the reactor core and SAM, a system analysis code that is based on the MOOSE framework and aims to enable fast-running whole-plant transient analyses with improved fidelity for various advanced reactor types, was used as a system model of the reactor's PCS and core. This example serves as a demonstration case for the compatibility and applicability of using a SAM-SCM coupled simulation to perform thermal-hydraulic analyses of microreactors.

3.1. Model Description

The SCM code was modified so as to be able to model MARVEL's unique core geometry, presented in Figure 17.

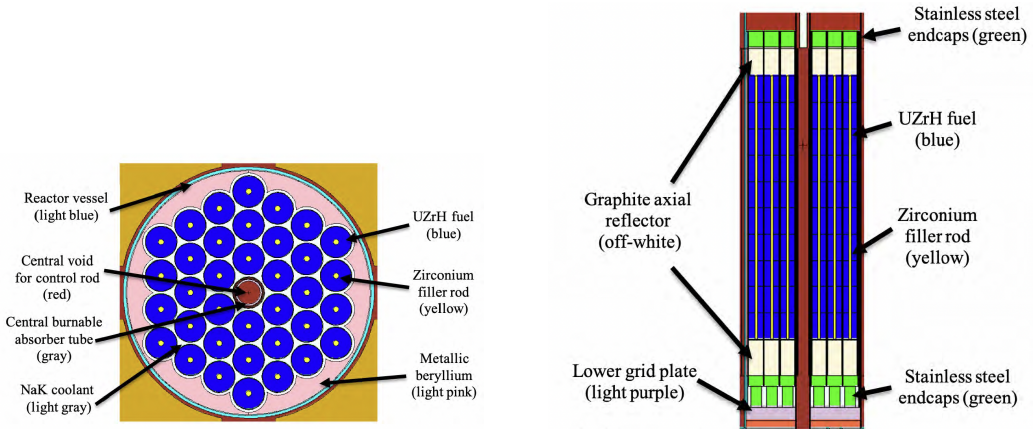

(a) Lateral cross section. (b) Axial cross section.

Figure 17. MARVEL core cross sections.

Compared to a "traditional" hexagonal, ducted sub-assembly with fuel pins in a triangular lattice, the MARVEL core only differs in the shape of the peripheral subchannels, since instead of straight flat sides, the MARVEL core sides conform to the circular shape of the peripheral fuel pins, allowing for a small gap. The SCM modification consists of creating a couple of new, custom Initial Conditions objects that calculate the modified surface area and wetted-perimeter of the peripheral subchannels.

This work leveraged the SAM model described in [12]. The SAM model, a diagram of which is shown in Figure 18, uses a single flow channel for the core and reflector regions, coupled with a heat structure to represent the fuel rods. It included all the major components of the PCS, with all four loops being explicitly modeled. The secondary side of the heat exchanger was modeled using a flow channel and inlet/outlet boundary conditions. Note that this model's use of lead as the secondary coolant was changed to gallium-indium-tin (eGa-In-Sn) in the latest version of the MARVEL design.

Coupling between the SCM and SAM codes for multiscale modeling of MARVEL was achieved through

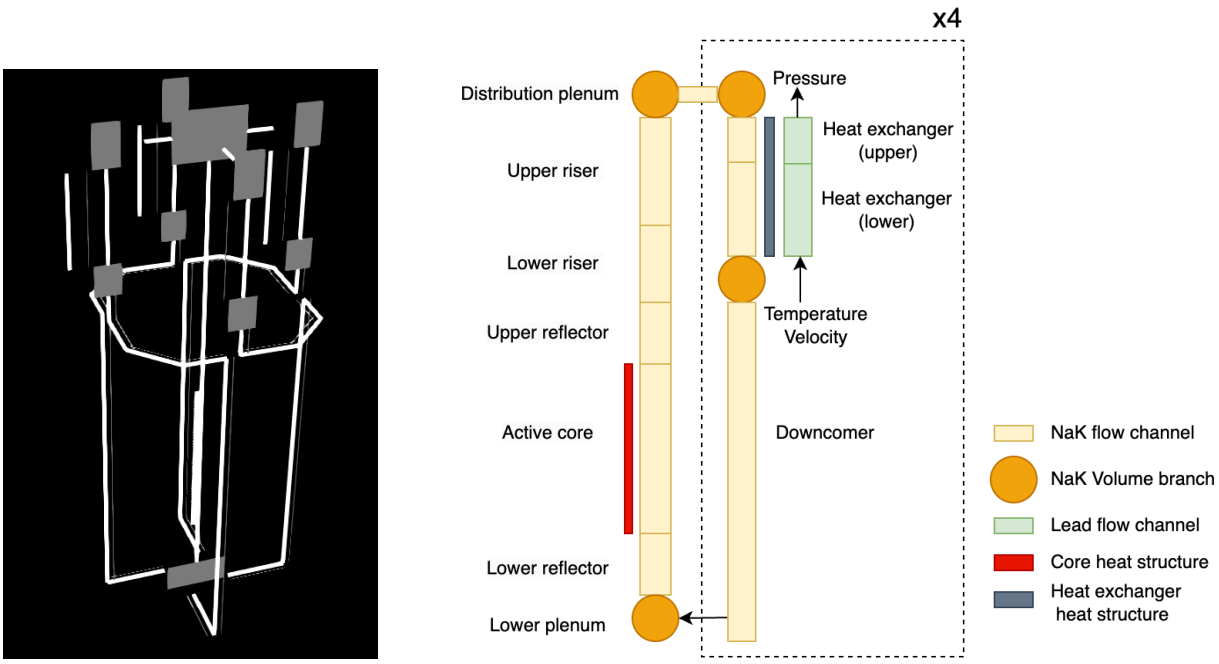

(a) 3D rendering of the SAM model (b) Diagram of the SAM model

Figure 18. SAM model of the MARVEL primary loop [12].

a domain overlapping approach in which SCM models the core, including the top and bottom reflectors, and SAM models the entirety of the system. SAM was the main application driving the transient analysis, whereas SCM operated as a sub-application running in steady state. Running SCM in steady state increased the computational efficiency without compromising accuracy, since the NaK coolant can be considered incompressible.

The coupling was implemented seamlessly out of the box—without requiring any additional coding—by utilizing the Multi-app functionality in MOOSE, post-processor transfers, and the built-in capability of the SAM flow channel component to derive a friction factor based on a user-specified pressure gradient. Users simply need to activate the coupling scheme and define the transferred quantities between the two codes. More specifically, SAM sends to SCM the mass flux and coolant temperature at the inlet of the core, along with the pressure at the outlet of the core. After its solve, SCM returns the pressure drop across the core. SAM calculates the required pressure gradient for the core component by dividing the pressure drop by the core length, and a friction factor is computed internally in SAM to match the pressure gradient. For transient calculations, it is important to account for the thermal inertia in the fuel pins. Since the fuel pins are not included in the SCM model, the power to the fluid during the transient is calculated by the SAM model, which includes heat structure modeling for the fuel pins. In future work, the fuel pins will be modeled by a specific BISON model and the power to the fluid will be transferred from BISON to SCM on a pin-by-pin basis. For each time step, fixed point iterations are performed. This is necessary for this natural convection loop because the pressure drop in the core and the mass flow rate in the loop are interdependent on each other.

3.2. Results

A startup-transient coupled SAM-SCM simulation was run. Power was assigned to the fuel pins, and natural circulation flow was initiated in the core and the loop before reaching steady state. The pressure drop across the core and the mass flux at the core inlet are plotted in Figure 19, demonstrating that the pressure

drop calculated by the SCM model is properly transferred and applied in the SAM model.

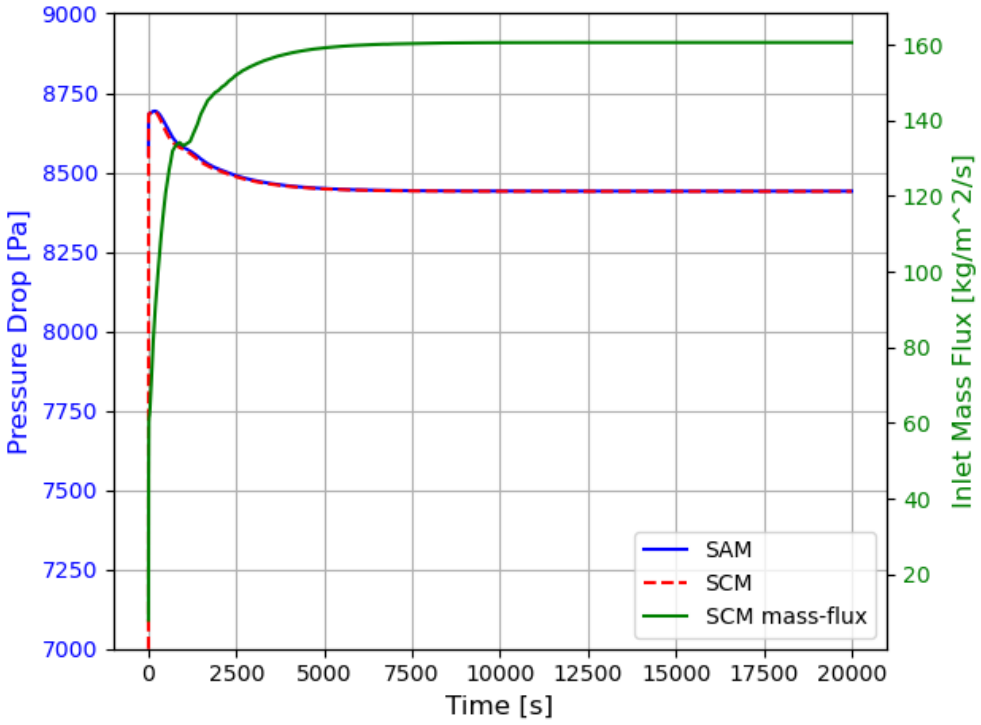

Figure 19. Pressure drop across the heated core (left axis) and the mass flux at the core inlet (right axis) for a coupled simulation.

A visualization of the coolant temperature field of the coupled SAM-SCM simulation at steady state is given in Figure 20a. The temperature distribution at the core exit is shown in Figure 20b. The coolant temperature is hotter between the first and second pin ring in the core as compared to the center and the reflector region. This demonstrates SCM's capability to better predict hot spots within the core in comparison to the simpler SAM model.

Table 6 compares the steady-state results obtained via the SAM standalone model, the SAM-SCM coupled model and the RELAP5-3D model developed by the MARVEL design team within the Microreactor Program. Overall, the SAM results and RELAP5-3D results are close to each other. The core inlet temperature is a little bit higher for the SAM model, but this will be further adjusted by refining the heat exchanger model.

Table 6. Comparisons of key quantities. The RELAP5-3D values are reported from [18].

	SAM standalone	Coupled SAM-SCM	RELAP5-3D
Core mass flow rate [kg/s]	1.43	1.52	1.53
Core inlet temperature [K]	744	745	738
Core outlet temperature [K]	811	809	805
Core pressure drop [Pa]	8462	8441	Not published

The evolution of the core mass flow rate and inlet/outlet core temperatures, for both the SAM standalone and SAM-SCM coupled models, is shown in Figure 21. The mass flow rate is higher in the coupled model than in the standalone one, meaning that the friction factor calculated by SCM is lower than that calculated by

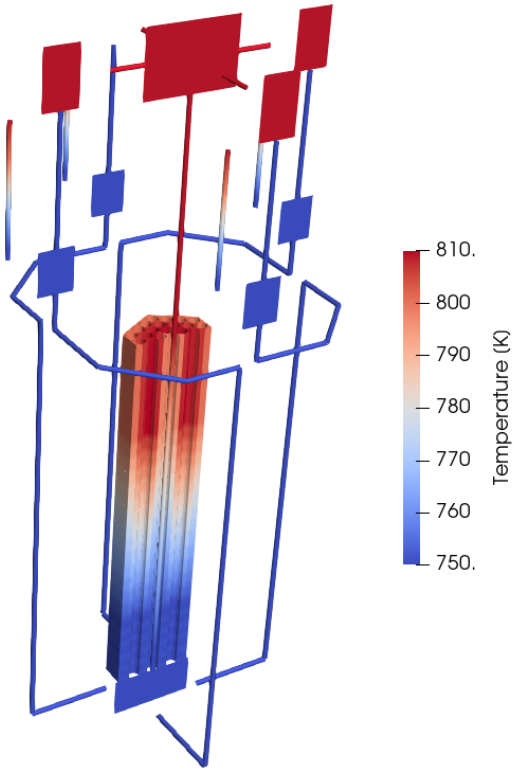

(a) Temperature distribution for the coupled model.

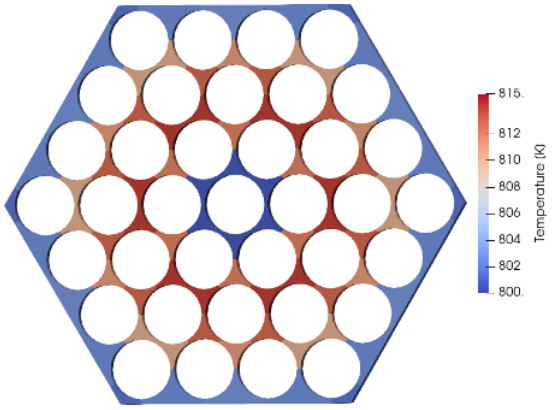

(b) Temperature distribution at the core outlet.

Figure 20. Coolant temperature distribution at steady state.

the SAM standalone model. Note that although both models use the Cheng-Todreas correlations, the SAM standalone model only has one channel for the whole core, while SCM calculates the friction factor for each individual subchannel. This results in a slightly lower temperature rise in the core for the coupled model.

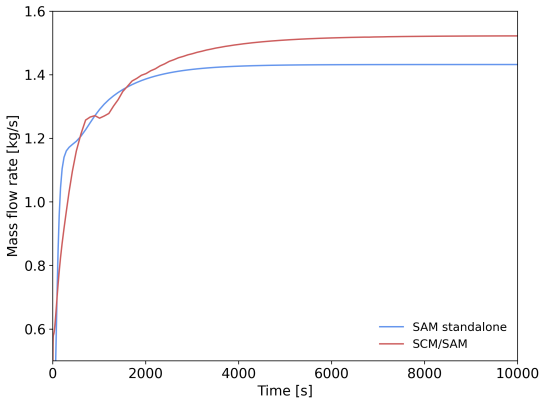

(a) Core mass flow rate

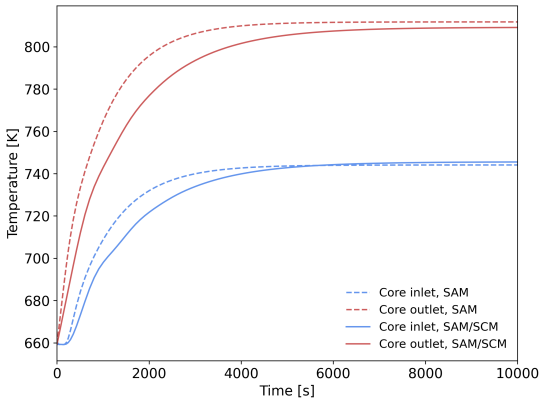

(b) Core inlet and outlet temperature

Figure 21. Core mass flow rate and temperature during the startup transient.

4. CONCLUSIONS

The recent long-duration sodium heat pipe experiment at SPHERE was used to validate the NEAMS heat pipe code Sockeye. The first 10 hours of this experiment involved startup of the heat pipe from a frozen state, which is a challenging regime to model due to the low pressure and temperature inside the heat pipe. Several models of the experiment were created, including different heat pipe models and different cooling models. The LCVF heat pipe model proved greatly superior to the Conduction heat pipe model, due to the mechanistic vapor modeling in the former. The calorimeter, which consisted of a tube coiled around the heat pipe axis, was greatly approximated due to its geometrical complexity in order to avoid the use of a 3D model. The most complex approximation of the calorimeter, in which the cooling fluid was modeled with a 1D flow channel, proved the most accurate of the cooling models considered. When the experimentally estimated calorimeter power was used directly, the cooling was believed to be underestimated, and the resulting simulation predicts much hotter heat pipe temperatures. With the best model of the experiment, the transient was decently matched by Sockeye. The condenser temperature values were much lower than in the adiabatic section, suggesting the possibility of effects such as pooling of excess working fluid and the presence of non-condensable gases. The heat pipe was designed without non-condensable gases, but including a small amount of non-condensable gas in the model improved the condenser temperature value predictions. However, this may just be a coincidental effect due to other effects and physics not captured by the numerical model. In addition to the challenges faced by needing to simplify the geometry, other challenges arose due to uncertainty in important physical properties such as thermal conductivity and emissivity—to which results are, unfortunately, quite sensitive. Furthermore, the thermocouple measurements in the experiment, particularly those in the evaporator section, were believed to have significant error as a result of wire-tying the thermocouples to the heat pipe instead of welding them to it. In response to the difficulties encountered in this validation exercise, the Sockeye team is providing feedback to the SPHERE team so as to improve future experiments. The SPHERE team is currently rebuilding the experimental setup used in this work with welded thermocouples to eliminate this source of error, so new experimental data may be available in January 2025. Another suggestion made to the SPHERE team was to include additional thermocouples—specifically, one on the inner or outer surface of the sanitary tube in each section (evaporator, adiabatic, and condenser)—which would be very useful for understanding where heat is being lost, as this is perhaps the most important data to consider in order to accurately model a complex system such as this.

A multiscale thermal hydraulics model of the MARVEL PCS was developed using SCM for the core and SAM for the loop. SAM and SCM exhibit the synergy expected from the fact they are both MOOSE-based applications. The coupling was achieved without any additional coding. The fact that the subchannel simulation provides a more detailed distribution of the coolant temperature in the core will increase the accuracy in detecting potential hot spots within the core. Future work will focus on integrating this coupled SAM-SCM approach with the MARVEL multiphysics model developed by the Micro-Reactor Applications Drivers area within the NEAMS program. This coupling methodology will also be applied to model the Primary Cooling Apparatus Test so as to validate this approach.

Page intentionally left blank

5. REFERENCES

[1] A. Faghri, *Heat Pipe Science and Technology*. Global Digital Press, second ed., 2016.

[2] D. A. Reay, P. A. Kew, and R. J. McGlen, *Heat Pipes: Theory, Design and Applications*. Elsevier Ltd., sixth ed., 2014.

[3] G. Giudicelli, A. Lindsay, L. Harbour, C. Icenhour, M. Li, J. E. Hansel, P. German, P. Behne, O. Marin, R. H. Stogner, *et al.*, "3.0-moose: Enabling massively parallel multiphysics simulations," *SoftwareX*, vol. 26, p. 101690, 2024.

[4] R. Martineau, D. Andrs, R. Carlsen, D. Gaston, J. Hansel, F. Kong, A. Lindsay, C. Permann, A. Slaughter, E. Merzari, R. Hu, A. Novak, and R. Slaybaugh, "Multiphysics for nuclear energy applications using a cohesive computational framework," *Nuclear Engineering and Design*, vol. 367, p. 110751, 2020.

[5] C. Matthews, V. Laboure, M. DeHart, J. Hansel, D. Andrs, Y. Wang, J. Ortensi, and R. C. Martineau, "Coupled multiphysics simulations of heat pipe microreactors using DireWolf," *Nuclear Technology*, vol. 207, no. 7, pp. 1142–1162, 2021.

[6] J. E. Hansel, R. A. Berry, D. Andrs, M. S. Kunick, and R. C. Martineau, "Sockeye: A one-dimensional, two-phase, compressible flow heat pipe application," *Nuclear Technology*, vol. 207, no. 7, pp. 1096–1117, 2021.

[7] J. Hansel, J. Hartvigsen, P. Sabharwall, L. Ibarra, and B. Feng, "Sockeye validation support using the SPHERE facility," in *International Conference on Physics of Reactors (PHYSOR)*, (Pittsburgh, PA), American Nuclear Society, May 2022.

[8] J. E. Hansel, C. da Silva Bourdot Dutra, L. Charlot, and E. Merzari, "The liquid-conduction, vapor-flow heat pipe model in sockeye," *Nuclear Engineering and Design*, vol. 426, p. 113359, 2024.

[9] P. Sabharwall, J. Hartvigsen, T. Morton, Z. Sellers, and J. S. Yoo, "SPHERE assembly and operation demonstration," Tech. Rep. INL/EXT-20-60782, Idaho National Laboratory, December 2020.

[10] Z. D. Sellers, T. Neumann, J. Hartvigsen, and P. Sabharwall, "Single primary heat extraction and removal emulator (SPHERE) long duration testing," Tech. Rep. INL/RPT-24-05019, Idaho National Laboratory, 2024.

[11] DOE, "New marvel project aims to supercharge microreactor deployment." https://www.energy.gov/ne/articles/new-marvel-project-aims-supercharge-microreactor-deployment. Accessed: 2024-12-11.

[12] S. Terlizzi and L. Charlot, "Towards a NEAMS-based high-fidelity model of the MARVEL reactor," Tech. Rep. INL/RPT-24-80887, Idaho National Laboratory, September 2024.

[13] R. Hu, L. Zou, D. O'Grady, T. Mui, Z. J. Ooi, G. Hu, E. Cervi, G. Yang, D. Andrs, A. Lindsay, *et al.*, "SAM: A Modern System Code for Advanced Non-LWR Safety Analysis," *Nuclear Technology*, 10 2024.

[14] V. Kyriakopoulos, M. E. Tano, and J. C. Ragusa, "Development of a single-phase, transient, subchannel code, within the moose multi-physics computational framework," *Energies*, vol. 15, no. 11, p. 3948, 2022.

[15] V. Kyriakopoulos, M. E. Tano, and A. Karahan, "Demonstration of pronghorn's subchannel code modeling of liquid-metal reactors and validation in normal operation conditions and blockage scenarios," *Energies*, vol. 16, no. 6, p. 2592, 2023.

[16] M. Tano, V. Kyriakopoulos, J. McCay, and T. Arment, "Validation of Pronghorn's subchannel code using EBR-II shutdown heat removal tests: SHRT-17 and SHRT-45R," *Nuclear Engineering and Design*, vol. 416, p. 112783, 2024.

[17] "Ceramic fiber heaters." https://www.watlow.com/products/heaters/high-temperature-heaters/ceramic-fiber-heaters. Accessed: 2024-12-11.

[18] C. Parisi and Y. Arafat, "MARVEL Thermal-hydraulics: Normal and Accidental Conditions," in *ANS Transactions*, 2022. American Nuclear Society Winter Meeting.